Mechanical Removal and Rescreening of Local Screening Charges at Ferroelectric Surfaces

Sheng Tong (童盛),[1] Woon Ik Park,[2] Yoon-Young Choi,[2] Liliana Stan,[1] Seungbum Hong,[2,*] and Andreas Roelofs[1,†]

[1]*Nanoscience and Technology Division, Argonne National Laboratory, Lemont, Illinois 60439, USA*
[2]*Materials Science Division, Argonne National Laboratory, Lemont, Illinois 60439, USA*

We report the kinetics of screening charge removal and rescreening on periodically poled lithium niobate using charge-gradient microscopy and electrostatic force microscopy (EFM). A minimum pressure needs to be applied to initiate mechanical screening charge removal, and increasing the pressure leads to further removal of charge until a threshold is reached when all screening charges are removed. We fit all rescreening EFM contrast curves under various pressures into a universal exponential decay. The findings imply that we can control the screening degree of ferroelectric surfaces by mechanical means without affecting the polarization underneath.

I. INTRODUCTION

Screening charges shield the electric field from the unbalanced bound polarization charges or other trapped charges until they are completely compensated. They are of great importance in many systems like piezoelectric actuators, ferroelectric thin films, colloid suspensions, solar batteries, and semiconductor devices [1–6]. In ferroelectrics, open circuit surfaces reach the ground state by either surface relaxation (internal screening) or adsorption (external screening). Internal screening will be observed only in ultrahigh vacuum, and for most applications ambient conditions lead to external screening. For example, the adsorption on oxide surfaces can be tuned by polarization switching [4,5], and, on the other hand, the chemical environment can control the ferroelectric polarization orientation [6].

In order to characterize the screening charges and the underlying polarization charges of ferroelectric materials, piezoresponse force microscopy (PFM), Kelvin-probe force microscopy (KPFM), and electrostatic force microscopy (EFM) are widely used [7,8]. To date, two different methods have been employed to manipulate screening charges on ferroelectric surfaces. The first is to vary the polarization by changing the temperature and making use of the pyroelectric properties [8,9]. The second is to inject charges onto the ferroelectric surfaces by applying a bias via a conductive atomic force microscopy (AFM) probe [10,11]. Consequently, EFM or KPFM is then used to monitor the local charge adsorption on the ferroelectric surface. Yet there are inherent issues in separating screening charges from polarization charges: It is known that the

*Corresponding author.
hong@anl.gov
†Corresponding author.
aroelofs@anl.gov

adsorption rate (k) is temperature dependent [1], and applying a bias over the coercive voltage switches the ferroelectric polarization and induces a depolarization field by injecting charges into the ferroelectric domains and domain walls [12,13]. In addition, none of the methods can fully remove the screening charges and establish the fully unscreened state, which would be the "real" time zero in the adsorption kinetics [1]. We address this issue by employing charge-gradient microscopy (CGM), which can measure the displacement currents at the domain wall boundaries of the ferroelectrics in contact mode by using a grounded conductive AFM probe (CGM probe), efficiently remove screening charges by mechanical means, and measure the collected charges during the process [14]. We demonstrate well-controlled mechanical removal of the external screening charges on the surface of a periodically poled lithium niobate (PPLN) and lead zirconate titanate (PZT) thin films and investigate the rescreening kinetics subsequently.

II. RESULTS AND DISCUSSION

To investigate the local screening charge removal and rescreening on the PPLN surface, we design the experimental sequence as shown in Fig. 1(a). First, we conduct an AFM and PFM scan to record the initial surface morphology and the ferroelectric domain configuration with a well-established method. The EFM scan is used to monitor the amount of screening before and after the CGM scan. In a fully screened state, the variation of the surface potential and surface potential gradient is much smaller than those in an unscreened state [8,9,15,16]. Before the CGM experiment, the EFM signals do not show significant contrast, as shown in Fig. 1(d). After performing the CGM imaging [Fig. 1(e)], it is evident from the subsequent EFM measurement [Fig. 1(f)] that screening charges have been removed by the CGM scan and the stray electric fields are now detectable, revealing the stripe domains in PPLN. The asymmetric EFM phase on positive and negative polarization domains
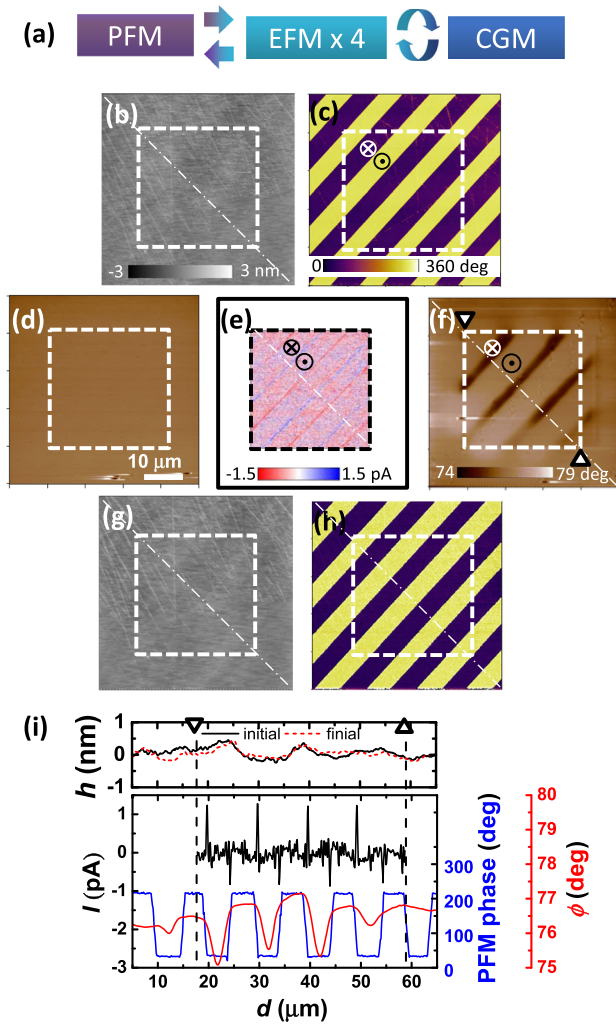
FIG. 1.   Mechanical removal of surface charges. (a) Schematic of experimental sequence; (b), (g) initial and final topography images of PPLN; (c), (h) initial and final PFM phase images; (d), (f) EFM phase images measured before and after the CGM scan; (e) CGM current; (i) line profile of the height (b), (g), EFM phase (f), CGM current (e), and PFM phase (h).

may be due to the domain orientation-dependent desorption energy [5,6,17,18].

Figures 1(g), 1(h), and S1 [19] prove that neither the topography nor the polarization of the PPLN has changed during the measurements. In order to study the screening charge removal process in more detail, the CGM measurements are repeated by using a variety of different forces as well as scan speeds on the same area after the surface is again rescreened and no EFM contrast is detected. Finally, an AFM and PFM measurement is conducted to confirm that the surface morphology and the ferroelectric polarization are unchanged. We correct the sample drift, which occurs during the measurements by comparing the initial and final AFM and PFM images. Note that the dashed squares in Figs. 1(b)–1(h) represent the CGM scanning area.

As shown in Figs. 1(b) and 1(g), the initial and final topography show no surface damage even though a

pressure of up to approximately 450 MPa is applied, which is also seen in the line profiles in Fig. 1(i) before and after CGM. The average roughness (R_a) in Figs. 1(b) and 1(g) are 0.28 and 0.21 nm, respectively. In Fig. 1(i), the current spikes of the CGM signal match well with the PFM phase boundaries; e.g., positive polarity is observed where the PFM phase changes from 210° to 30°.

The contrasts in Fig. 1(f) further extend over the scanned range, which is due to the high speed of the CGM scanning and the way the AFM achieves reliable topography acquisition. The AFM scanner overscans the range of the region set by the parameter we input to achieve the uniform speed in the scan range. Thus, the outer acceleration and deceleration scanning leaves the wider domain patterns in the EFM image. One may note that such movement leaves wider domain patterns in the fast scan direction but not in the slow one.

More CGM experiments varying the number of lines in the slow scan axis over the same area did not reveal any significant difference in the CGM images. This result indicates that the rate of charge removal is independent of the spacing over the range of line spacing we use. However, it should be noted that, if the space between each line scan is much larger than the tip diameter, the width of removal is limited to the trace of the tip [20].

As shown in Fig. 2, we conduct a set of experiments on 90-nm-thick PZT (20/80) thin films deposited on $SrRuO_3/SrTiO_3$ substrates where the domain patterns are written during which excess charges are deposited to the PZT surface. Figures 2(a) and 2(b) illustrate the smooth PZT films ($R_a = 0.28$ nm) consist of bottom to top domains as deposited. After we write the +8 and −8 V patterns, as in Fig. 2(c), we observe the overscreened surface by using EFM, similar to the previous reports
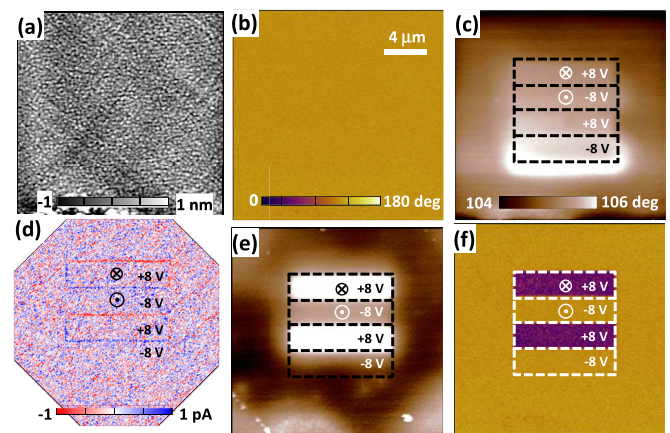

FIG. 2.   Evidence for removal of the injected charges on PZT thin films using CGM. (a) PZT topography, (b) PFM phase before, and (c) EFM phase after selective charge injection by biasing the tip with −8 and 8 V. (d) CGM after the EFM measurement in (c). (e) EFM phase after the CGM scan in (d). (f) PFM phase of the domain writing pattern.

[9,10,15,21]. By conducting CGM on the same region [Fig. 2(d)], we observe by using EFM the opposite charge polarity to that of the injected ones, which further confirms that the surface charges are removed instead of created or injected.

The screening charges tend to neutralize the polarization charges of ferroelectric materials [8], as illustrated in regime I of Fig. 3(c), which minimizes the variation of surface potential above the stripe domains. Thus, the initial EFM phase image displays no contrast related to the domain pattern, indicative of surface potential variation resulting in a smaller electric field gradient than the resolution of EFM. During the CGM imaging, we apply a sufficiently large force to remove the screening charges without affecting the polarization underneath, leading to a strong potential gradient built up between up and down domains as shown in regime III of Fig. 3. This gradient is evidenced by the subsequent EFM image.

As we find that CGM could remove the screening charges from ferroelectric surfaces and detect the local surface potential gradients, we then further explore how the pressure applied to the probe and scan speed of the probe influence the rate of surface charge removal and the kinetics of rescreening.

Figure 3(a) shows the contrasts of the CGM current and EFM phase shift as a function of applied pressure. The EFM contrast ($\Delta\phi$) and CGM contrast (ΔI) vs pressure (P) are plotted in Fig. 3(a). The contrast is defined as the difference between the maximum and minimum peaks, and the pressure is obtained by estimating hemispherical tip contact areas with a radius of 45 and 100 nm for the Pt-wired probe and Ir-coated Si probe, respectively.

Figure 3(a) can be divided into three regimes, marked by two parameters, the threshold pressure (P_{th}) and the critical pressure (P_{crit}): In regime I where $P < P_{th}$, $\Delta\phi$ and $\Delta I \approx 0$, the CGM tip cannot remove screening charges; in regime II where $P_{th} < P < P_{crit}$, $\Delta\phi$ and ΔI are proportional to the applied pressure P, implying that the CGM tip can partially remove screening charges and the removal rate is directly proportional to the applied pressure; in regime III where $P > P_{crit}$, $\Delta\phi$ and ΔI are maximized, indicating that the screening charge is removed completely. The EFM phase shift is sensitive to the electric field gradient, which scales with the gradient of the net surface charges (ΔQ) for the same geometry [8,15]. As we use stiff cantilevers, we can assume that $\Delta\phi$ scales linearly with ΔQ. As ΔI is proportional to the rate of ΔQ and the CGM scan speed is kept constant at 600 μm/s for all measurements, we expect that ΔI scales linearly with $\Delta\phi$, which is confirmed in Fig. 3(b). The above discussion suggests three distinct regimes for CGM measurements which are depicted in Fig. 3(c): (I) below P_{th}, no CGM current is detected as the polarization charge is fully screened and screening charges cannot be removed; (II) the CGM current scales with the applied pressure as the CGM tip partially removes the screening charges; (III) the CGM current is saturated once the tip can fully remove the surface charges.

We assume that the screening charges are fully removed at high pressure applied on the CGM probe during the scan for the following reasons. First, as the surface potential scales with the degree of screening, the surface potential variation after CGM scans measured by using KPFM after at least 2 min is approximately 2.4 V on PPLN (Fig. S2) [19], which is 6 times larger than the fully
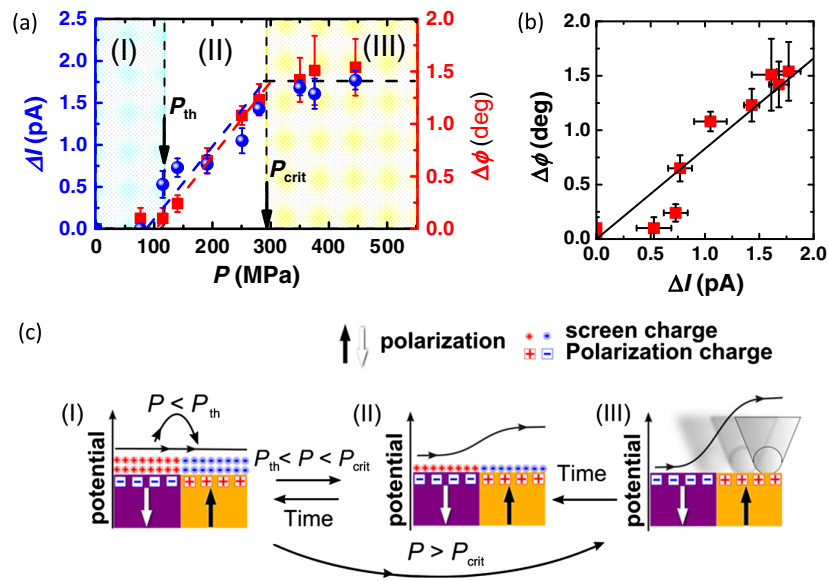

FIG. 3.   Effect of applied pressure on surface charge removal. (a) CGM contrast (ΔI) and EFM contrast ($\Delta\phi$) as a function of applied pressure (P); (b) correlation between ΔI and $\Delta\phi$; (c) schematic illustration of surface charge removal and rescreening in different regimes of the (I) fully screened surface, (II) partial screened surface, and (III) unscreened surface.

screened surface [8,9]. Second, we show [14] that the scraped charges per area are close to $2P_r$, indicating that we are scraping most, if not all, of the screen charges on the surface.

Time-dependent EFM measurements are carried out to investigate the rescreening process after CGM scans. Figure 4(a) shows the dependence of $\Delta\phi$ decay as a function of time on the applied pressure. At time 1 min, $\Delta\phi$ strongly depends on the applied pressure, where a larger pressure is associated with a larger $\Delta\phi$. However, $\Delta\phi$ reaches a minimum after about 7 min, where $\Delta\phi$ was almost the same regardless of the initial applied pressure during the CGM measurement.

To quantify the kinetics of the rescreening, as shown in Fig. 4(b), we approximate the time dependence of EFM contrast by using an exponential decay function based on the following deductions. As the most polar composition in the atmosphere, water is the primary screening species [4,16,22]. By assuming that the rescreening is a first-order adsorption, with Elovich's equation and Lagergren's equation [23] as

(a)

(b)

(c)

FIG. 4. Surface charge rescreening after mechanical removal. (a) $\Delta\phi$ decay after CGM scans under various pressures (P); (b) universal $\Delta\phi$ decay fitted by using Eq. (3), and elapsed time (t_0) vs P; (c) screened percentage (S) vs P.

$$\frac{d\theta}{dt} = k(1-\theta), \qquad (1)$$

where θ is the fraction of sites occupied by the charge carriers at time t (the ferroelectric surface is unscreened at $t = 0$) and k is the adsorption rate, we can integrate Eq. (1) to yield

$$1 - \theta = \exp(-kt) \propto \sigma_{\text{net}}, \qquad (2)$$

where σ_{net} is the net surface charge density. Since $\Delta\phi$ is proportional to σ_{net}, and k is the reciprocal of the adsorption half-life time τ, we can rewrite Eq. (2) to [9,10,15]

$$\Delta\varphi = \Delta\varphi_0 \exp\left(-\frac{t'}{\tau}\right), \qquad (3)$$

where $t' = t - t_0$, $\Delta\phi_0$ is a prefactor, and t_0 is a time constant. The t_0 is not negligible when the screening charges are not fully removed, which is the case when $P_{\text{th}} < P < P_{\text{crit}}$. By fitting the two independent variables τ and t_0 for all the EFM contrast decay curves in Fig. 4(a), we obtain a universal decay curve with τ of 2.37 min as seen in Fig. 4(b). We also observe a similar value of τ of 2.18 min by directly monitoring the surface potential decay within a KPFM scan (Fig. S2) [19]. With the τ value in approximately 2 min, we can infer that the adsorption is chemical in nature with adsorption energy in tens to hundreds of kJ/mol [1,5,17,18,23]. Usually, the screening process can be understood as follows: First, the water is physisorbed to the ferroelectric surface in picoseconds to milliseconds; second, water is partially self-ionized into H_3O^+ and OH^-; and third, the polar ions diffuse in the surface water layer and electrostatically screen the polarization charges underneath in a few to tens of minutes [1,15,22,24]. Because the physisorbed water does not screen the ferroelectric surface [1,16–18], and the physical desorption energy is much smaller than those of the chemisorbed H_3O^+ or OH^-, it is possible that not only the chemical bonding between the ions and polarization charges are broken mechanically but also the adsorbed water is pushed away due to the high scan speed during the CGM imaging.

We also consider other possible mechanisms such as mechanical wear or a pressure-induced surface piezoelectric potential that might lead to the same results we obtain. The simplest mechanism of removal of charged species is indeed mechanical wear where the tip tears the chemical bond between the surface layer and the bulk of the materials [25,26]. We observe the mechanical wear when we exert 40 μN of loading force to the conductive diamond-coated tip, where the topography of the CGM area shows distinct indentation [14]. Regarding the possibility of a pressure-induced surface piezoelectric potential, we calculate that the charge induced by such a potential is at least 2 orders of magnitude lower than what we measure [14]. Therefore, although we cannot exclude the existence of the
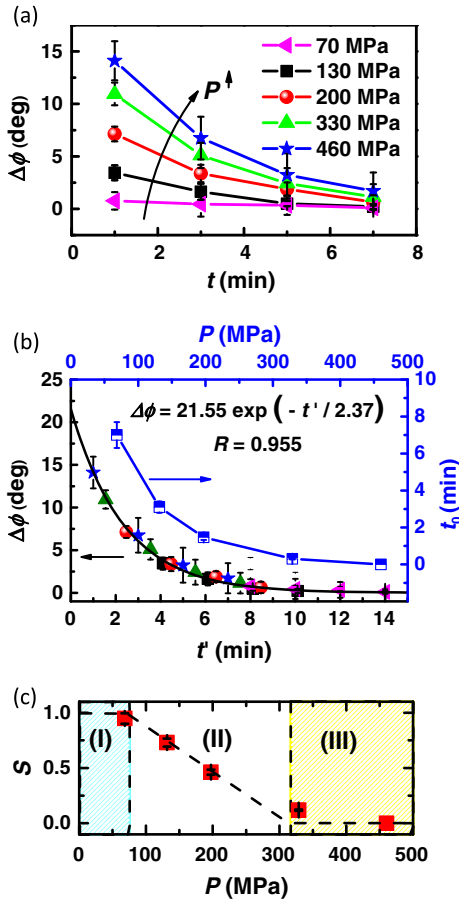
piezopotential, we believe it plays a minor role. Regarding the pressure effect on polarization dynamics, we note that those usually lead to nonvolatile effects, such as flexo-electric-effect-induced polarization switching from one polarization to the opposite one or pressure-induced phase transition from nonpolar phase to polar phase [27,28], which upon the removal of pressure will not return to the original state. However, in our case, as evidenced by Fig. 1, the periodically poled polarization pattern remains the same after the CGM imaging, which excludes those reversible but nonvolatile effects.

The rescreening kinetics is strongly affected by the adsorbed molecule and ion species, temperature, and moisture, while our experiments are done in ambient air with no control over the humidity. Nevertheless, the universal τ under various applied pressure suggests that we remove the surface charges without perturbing the driving force for the rescreening, which is a function of both the ambient condition and the net charges from the combination of the remaining screening charges, if any, and the polarization charges underneath. Noteworthy is that τ is different from that reported [9,10], possibly due to the difference in the temperature and moisture, the state of screening (e.g., overscreening), and the type of the ferro-electric materials used in other studies.

As seen in Fig. 4(b), a smaller P corresponds to a larger t_0, and vice versa. Based on Eq. (1), a bare ferroelectric surface is unscreened at $t = 0$, which implies that a finite t_0 corresponds to an effective elapsed time required for an unscreened surface to be rescreened to the initial screening state right after a CGM scan under a certain value of pressure (see Fig. S4) [19]. So a larger t_0 corresponds to a greater degree of screening, and the value is determined by the applied pressure during the CGM scans.

From the discussion above, we have shown that the surface charges rescreened in a manner of an exponential recovery. A common τ regardless of the applied pressure implies a universal rescreening behavior, while the applied force determines the starting point in the decay curve. We also know that the applied force determines the amount of the charge removal from Fig. 3. Thus, based on the definition of t_0 and exponential recovery nature of the rescreening, we can define the degree of screening as

$$S = 1 - \exp\left(-\frac{t_0}{\tau}\right), \tag{4}$$

where $S = 0$ for the unscreened surface and $S = 1$ for the fully screened surface. Similar to that of ΔI or $\Delta\phi$ vs P in Fig. 3(a), we find the plots of S vs P in Fig. 4(c). Obviously, we again find the three regimes: In regime I where $P < P_{th}$, $S \approx 0$; in regime II where $P_{th} < P < P_{crit}$, S linearly decreases with the increase of P; in regime III where $P > P_{crit}$, $S = 0$. By adopting Eqs. (3) and (4), we can quantitatively determine S and, thus, precisely control the amount of the charge removal during the CGM scan.
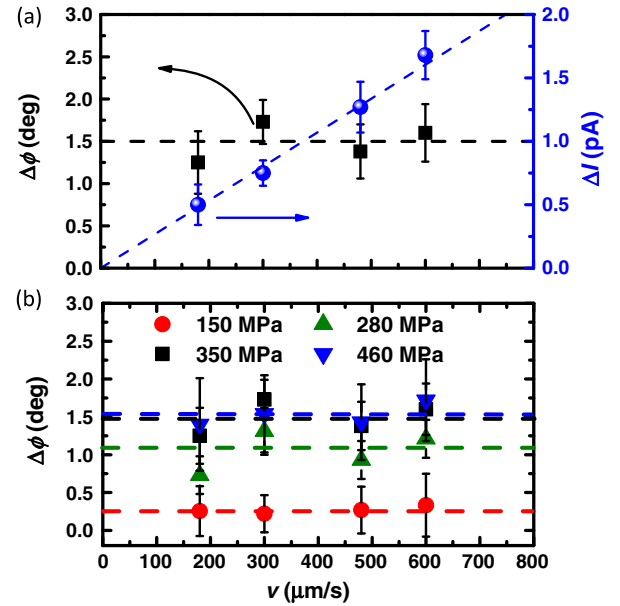

FIG. 5. Scan speed influence to local surface charge removal and current flow. (a) Scan-speed-dependent ΔI and $\Delta\phi$; (b) scan-speed-dependent $\Delta\phi$ after CGM scans under various pressures.

Figure 5 displays the influence of the scan speed of CGM on the screening charge removal process. The EFM phase images in Fig. S5 [19] imply that the total amount of the removed screen charge is the same, as shown in Fig. 5(a). Therefore, the amount of the charges collected by the AFM tip should linearly scale with the scan rate, which was confirmed in Fig. 5(a) [14]. The EFM contrast remains the same regardless of scan speed, however, varied with the applied pressure as shown in Fig. 5(b). This result implies that the amount of charges removed by the CGM probe is determined rather by the applied pressure and not primarily by the scan speed.

III. CONCLUSION

In summary, we study the local surface charge removal and rescreening on the PPLN surface by using a CGM probe. We find that the applied pressure is the primary factor that determines the amount of the removed screening charges while the CGM scan speed plays a minor role. The charge flow through the CGM probe is proportional to the magnitude of the removed screening charges. Unscreened polarization charges, which are exposed to the ambient, are rescreened in a matter of minutes following an exponential recovery with a universal half-life time τ of 2.37 min. These findings indicate that, with little impact on the ferroelectric polarization, we can control the degree of screening on a ferroelectric surface by a mechanical manner. Furthermore, our work opens up an interesting field of mechanochem-istry and its dynamics at the nanoscale, which can lead to tunable surface chemistry by creating a metastable charge state using local mechanical means.

[1] A. W. Adamson and A. P. Gast, *Physical Chemistry of Surfaces* (Wiley-Interscience, the University of Michigan, 1997), p. 808.

[2] M. Grätzel, Dye-sensitized solar cells, J. Photochem. Photobiol. C **4**, 145 (2003).

[3] M. Lannoo, C. Delerue, and G. Allan, Screening in semiconductor nanocrystallites and its consequences for porous silicon, Phys. Rev. Lett. **74**, 3415 (1995).

[4] Y. Yun and E. I. Altman, Using ferroelectric poling to change adsorption on oxide surfaces, J. Am. Chem. Soc. **129**, 15684 (2007).

[5] K. Garrity, A. M. Kolpak, S. Ismail-Beigi, and E. I. Altman, Chemistry of ferroelectric surfaces, Adv. Mater. **22**, 2969 (2010).

[6] R. V. Wang, D. D. Fong, F. Jiang, M. J. Highland, P. H. Fuoss, C. Thompson, A. M. Kolpak, J. A. Eastman, S. K. Streiffer, and A. M. Rappe, Reversible chemical switching of a ferroelectric film, Phys. Rev. Lett. **102**, 047601 (2009).

[7] S. Hong, in *Nanoscale Phenomena in Ferroelectric Thin Films*, edited by S. Hong (Springer, New York, 2004), p. 288.

[8] S. V. Kalinin and D. A. Bonnell, Local potential and polarization screening on ferroelectric surfaces, Phys. Rev. B **63**, 125411 (2001).

[9] S. V. Kalinin and D. A. Bonnell, Screening phenomena on oxide surfaces and its implications for local electrostatic and transport measurements, Nano Lett. **4**, 555 (2004).

[10] Y. Kim, M. Park, S. Bühlmann, S. Hong, Y. K. Kim, H. Ko, J. Kim, and K. No, Effect of local surface potential distribution on its relaxation in polycrystalline ferroelectric films, J. Appl. Phys. **107**, 054103 (2010).

[11] X. Q. Chen, H. Yamada, T. Horiuchi, K. Matsushige, S. Watanabe, M. Kawai, and P. S. Weiss, Surface potential of ferroelectric thin films investigated by scanning probe microscopy, J. Vac. Sci. Technol. B **17**, 1930 (1999).

[12] A. Roelofs, N. A. Pertsev, R. Waser, F. Schlaphof, L. M. Eng, C. Ganpule, V. Nagarajan, and R. Ramesh, Depolarizing-field-mediated 180° switching in ferroelectric thin films with 90° domains, Appl. Phys. Lett. **80**, 1424 (2002).

[13] S. Bühlmann, E. Colla, and P. Muralt, Polarization reversal due to charge injection in ferroelectric films, Phys. Rev. B **72**, 214120 (2005).

[14] S. Hong, S. Tong, W. Park, Y. Hiranaga, Y. Cho, and A. Roelofs, Charge gradient microscopy, Proc. Natl. Acad. Sci. U.S.A. **111**, 6566 (2014).

[15] S. V. Kalinin, C. Johnson, and D. A. Bonnell, Domain polarity and temperature induced potential inversion on the $BaTiO_3$ surface, J. Appl. Phys. **91**, 3816 (2002).

[16] A. Ievlev, S. Jesse, A. Morozovska, E. Strelcov, E. Eliseev, Y. Pershin, A. Kumar, V. Y. Shur, and S. Kalinin, Intermittency, quasiperiodicity and chaos in probe-induced ferroelectric domain switching, Nat. Phys. **10**, 59 (2014).

[17] D. Li, M. Zhao, J. Garra, A. M. Kolpak, A. M. Rappe, D. A. Bonnell, and J. M. Vohs, Direct in situ determination of the polarization dependence of physisorption on ferroelectric surfaces, Nat. Mater. **7**, 473 (2008).

[18] J. Garra, J. M. Vohs, and D. A. Bonnell, the effect of ferroelectric polarization on the interaction of water and methanol with the surface of $LiNbO_3$ (0001), Surf. Sci. **603**, 1106 (2009).

[19] See Supplemental Material at http://link.aps.org/supplemental/10.1103/PhysRevApplied.3.014003 for the detailed experimental procedure, PFM amplitude images of PPLN before and after the CGM scan, EFM and KPFM images of the time-dependent rescreening on the PPLN surface, CGM scan speed influence on the EFM phases of the PPLN surface, and more.

[20] Y. Kim, J. Kim, S. Bühlmann, S. Hong, Y. K. Kim, S.-H. Kim, and K. No, Screen charge transfer by grounded tip on ferroelectric surfaces, Phys. Status Solidi (RRL) **2**, 74 (2008).

[21] J. Kim, Y. Kim, K. No, S. Bühlmann, S. Hong, Y. Nam, and S. Kim, Surface potential relaxation of ferroelectric domain investigated by kelvin probe force microscopy, Integr. Ferroelectr. **85**, 25 (2006).

[22] F. Verniani, The total mass of the Earth's atmosphere, J. Geophys. Res. **71**, 385 (1966).

[23] M. Low, Kinetics of chemisorption of gases on solids, Chem. Rev. **60**, 267 (1960).

[24] T. Morimoto, M. Nagao, and F. Tokuda, The relation between the amounts of chemisorbed and physisorbed water on metal oxides, J. Chem. Phys. **73**, 243 (1969).

[25] K.-H. Chung, Y.-H. Lee, D.-E. Kim, J. Yoo, and S. Hong, Tribological characteristics of probe tip and PZT media for AFM-based recording technology, IEEE Trans. Magn. **41**, 849 (2005).

[26] K.-H. Chung, Y.-H. Lee, Y.-T. Kim, D.-E. Kim, J. Yoo, and S. Hong, Nano-tribological characteristics of PZT thin film investigated by atomic force microscopy, Surf. Coat. Technol. **201**, 7983 (2007).

[27] H. Lu, C. W. Bark, D. Esque de los Ojos, J. Alcala, C. B. Eom, G. Catalan, and A. Gruverman, Mechanical writing of polarization, Science **336**, 59 (2012).

[28] P. Zubko, G. Catalan, and A. K. Tagantsev, Flexoelectric effect in solids, Annu. Rev. Mater. Res. **43**, 387 (2013).